NANO LETTERS

Letter

pubs.acs.org/NanoLett

Experimental Proof of Concept of Nanoparticle-Assisted STED

Yannick Sonnefraud,*[,†,‡] Hugo G. Sinclair,[§] Yonatan Sivan,[∥] Matthew R. Foreman,[⊥] Christopher W. Dunsby,[§] Mark A. A. Neil,[§] Paul M. French,[§] and Stefan A. Maier[‡]

[†]Institut Néel, CNRS UPR 2940, 25 rue des Martyrs BP 166, 38042 Grenoble Cedex 9, France

[‡]Experimental Solid State Group and [§]Photonics Group, Imperial College London, Blackett Laboratory, SW7 2AZ London, United Kingdom

[∥]Unit of Electro-optics Engineering, Faculty of Engineering Science, Ben-Gurion University, P.O. Box 653, Beer-Sheva 8410501, Israel

[⊥]Max Planck Institute for the Science of Light, Laboratory of Nanophotonics & Biosensing, 91058 Erlangen, Germany

Supporting Information

ABSTRACT: We imaged core−shell nanoparticles, consisting of a dye-doped silica core covered with a layer of gold, with a stimulated emission depletion, fluorescence lifetime imaging (STED-FLIM) microscope. Because of the field enhancement provided by the localized surface plasmon resonance of the gold shell, we demonstrate a reduction of the STED depletion power required to obtain resolution improvement by a factor of 4. This validates the concept of nanoparticle-assisted STED (NP-STED), where hybrid dye-plasmonic nanoparticles are used as labels for STED in order to decrease the depletion powers required for subwavelength imaging.

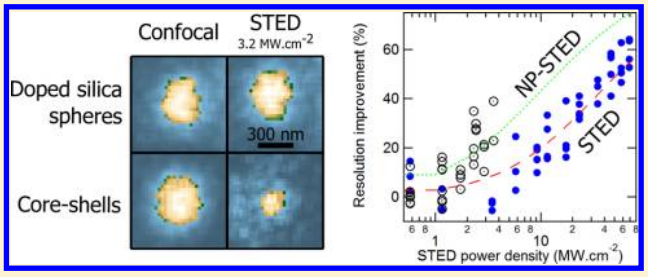

KEYWORDS: *Plasmonics, STED microscopy, nanoshells, fluorescence, microscopy*

For close to two decades, the diffraction limit has not been the ultimate bound to resolution in far-field fluorescence microscopy. Indeed, several techniques using some particular physical properties of nanoemitters of light have demonstrated far-field resolutions in the nanometer range, giving birth to several "nanoscopies". STimulated Emission Depletion microscopy (STED) was the first type of nanoscopy to be proposed.[1] In this scheme, the object to be imaged is labeled with small fluorescent dyes or fluorescent proteins. The fluorescence of the labels is excited by a focused laser beam. An additional laser, at a wavelength tuned to the red-edge of the emission of the dye and with a doughnut shape at the focal plane, forces the emitters into their ground state via stimulated emission. This only leaves the emitters lying at the zero-intensity center of the doughnut in their excited state. The size of this volume of excited emitters is not limited by diffraction anymore. An image is reconstructed by raster scanning the sample with respect to the lasers, and this image has an effective resolution much below the diffraction limit, which now depends on the intensity of the STED laser with respect to the saturation intensity of the dyes used.

The first experimental demonstrations of the principles of STED presented a modest improvement of resolution.[2,3] Initially, a STED microscope required a powerful, pulsed laser to generate the depletion beam, which was confining the technique to specialized laboratories. Still, by the imaging of fluorescent labels attached to specific proteins in cells, it allowed for the understanding of some biological processes inaccessible without the enhanced resolution.[4,5] Following this, many developments have been made to simplify the experimental realization of the technique, such as the demonstration that it is possible to perform STED with continuous wave lasers,[6,7] or even low-cost diodes.[8] Time-gating the detected signal also allows the resolution to be optimized[9−12] and therefore provides a means to reduce the STED power. Following the work on STED, other nanoscopies have emerged based on stochastic switching of emitters to/from dark states combined with single molecule localization, for example, refs 13−20. Still, to this day, STED remains one of the most widely used nanoscopy methods as it is well-suited for dynamic imaging, with demonstrated live cell[21] or in vivo imaging.[22] So far, most of the developments in STED have focused on the technique itself and less on the production of fluorescent labels designed for STED.[21,23]

In parallel, the development of the field of plasmonics has yielded many advances in the manipulation of light at the nanometric scale. A surface plasmon polariton is a charge density wave at the interface between a metal and a dielectric, which can be excited by light—and in the case of noble metals, from the near-UV to the IR range.[24] Metallic nanoparticles can exhibit localized surface plasmon resonances (LSPRs),

Received: April 16, 2014
Revised: July 18, 2014
Published: July 22, 2014

   dx.doi.org/10.1021/nl5014103 | *Nano Lett.* 2014, 14, 4449−4453

collective electronic oscillations which give rise to interesting properties.[25] LSPRs enhance the electromagnetic field locally in subwavelength volumes, which can be used to increase the efficiencies of spectroscopic methods such as Raman scattering[26] or surface-enhanced infrared absorption (SEIRA).[27] Metal NPs can also act as nanoantennas, effective transducers between the far field and the near field: at the LSPR, their scattering cross section can be much larger than their physical cross section, which allows them to efficiently capture light. This light is then concentrated in the vicinity of the nanoparticle.[28] Conversely, nanoantennas can modify the radiative properties of nanoemitters placed in their vicinity, assisting for instance the emitter in coupling its energy to the far field: fluorescence enhancement by several orders of magnitude has been demonstrated.[29] The spectral position of the LSPRs can be tuned by changing the shape, size, and material of the NPs used.

Plasmonics is finding an increasing number of applications,[30] and it is using the knowledge acquired in that field that we proposed to use hybrid labels to perform STED: a fluorescent element combined with a plasmonic resonator, nanoparticle-assisted STED, NP-STED.[31−33] Indeed, in its simplest form (i.e., for pulsed STED), the resolution Δr achievable in STED can be described by the functional form $\Delta r \approx \lambda/[2\mathrm{NA}(1 + I_{\mathrm{STED}}/I_{\mathrm{sat}})^{1/2}]$, with λ the wavelength used, NA the numerical aperture of the objective, I_{STED} the intensity of the depletion beam at its crest, and I_{sat} the saturation intensity of the fluorescent emitter used. Increasing the intensity of the depletion beam directly increases the resolution. LSPRs are known to provide high field confinement and enhancement on deeply subwavelength volumes.[24,34] The STED resolution improvement can also be expressed as $\Gamma_{\mathrm{res}}^{\mathrm{STED}} \cong (1 + P_{\mathrm{STED}}/P_{\mathrm{sat}})^{1/2}$, with P_{STED} and P_{sat} the power of the depletion beam and the saturation power of the dye used, respectively. In earlier theoretical works[31,32] we have shown that when the STED dyes are combined with a plasmonic cavity, the resolution improvement becomes $\Gamma_{\mathrm{res}}^{\mathrm{NP\text{-}STED}} \cong [1 + \Gamma_{\mathrm{p}}(P_{\mathrm{STED}}/P_{\mathrm{sat}})]^{1/2}$, where Γ_{p} is the ratio of the average intensity enhancement provided by the plasmon resonance at the STED wavelength over the enhancement of decay rate of the dye.[31] Note that, for this reason, contrary to the majority of the work on LSPRs and fluorescence, we want to avoid modifying the emission properties of the emitter used, as this can be detrimental to the resolution improvement: an increase in fluorescence decay rate leads to a reduction of the saturation intensity and consequently to a reduction of the STED resolution.[31] The modification in decay rate is linked to the field enhancement at the level of the dye, at the wavelength of emission.[28] In NP-STED, the change in decay rate is mitigated by using plasmonic resonances red-shifted compared to the emission of the dye, thus minimizing the field enhancement at the emission wavelength, and enhancing the field mostly at the depletion wavelength. Then, by providing the enhancement factor Γ_{p}, the plasmonic cavity should allow to reach STED superresolution with smaller depletion powers than that required with standard labels or, at constant depletion power, improve the resolution achievable. Somewhat similarly, it was already suggested theoretically to use the effect of stimulated emission in the context of structured-illumination imaging.[35] However, an experimental demonstration of resolution improvement/intensity reduction was not demonstrated so far, especially not in three dimensions. In this article we present a proof of principle experimental demonstration that 3D NP-STED labels can allow subdiffraction resolutions in STED to be reached, with a depletion intensity four times lower than that required for the same fluorescent label without the help of a plasmonic resonator.

The hybrid NPs chosen for this work consist of core−shell structures: the dielectric core containing the fluorescent emitters is covered with a thin shell of gold. The core−shell system has been extensively studied, and the position of its plasmon resonance can be tuned by changing the dimensions of the shell. An increase of inner diameter leads to a red-shift of the LSPR, while making the shell thicker leads to a blue-shift of the resonance, at constant inner diameter.[37] Moreover, it has been shown that, in a core−shell configuration, the dyes embedded in the cores experience a field enhancement that is mostly homogeneous, independent of their position or of the relative position of the core−shell with respect to the depletion beam.[38] The NPs are produced in two steps. First, cores of radius r_{core} = 60 nm are chemically grown in an aqueous colloidal solution and consist in silica spheres doped with ATTO 647N,[39] a fluorescent dye commonly used in STED emitting around 670 nm.[9] An estimate of the number of dye molecules has been made by the manufacturer of the cores (Hybrid Silica Technologies). It is based on the comparison of the emitted intensity from a single ATTO 647N dye molecule in water with the total emission of one single core and yields 25 dye molecules per particle. One part of the solution is kept to be used as reference in the estimation of the resolution improvement. The rest of the cores are then subjected to the chemical growth of a gold shell (Growth performed by Nanocomposix).[37] Figure 1a presents a transmission electron

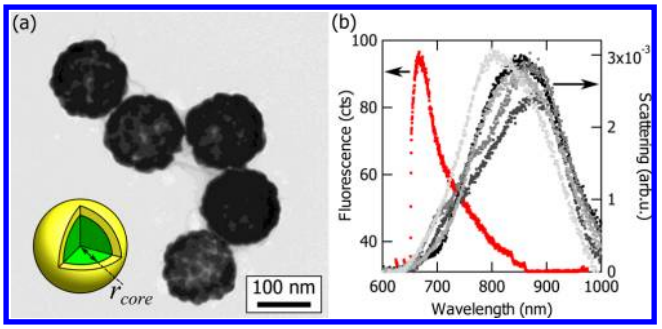

Figure 1. Hybrid NP-STED nanoparticles (NPs). (a) TEM image of the hybrid NP consisting of a dye-doped silica core of radius r_{core} = 60 nm coated with a 20 nm gold shell. Inset: sketch of the core−shells used. (b) Red curve: fluorescence spectrum emitted by the NPs, corresponding to the typical emission of the ATTO 647N dye doping the core. Gray curves: scattering spectra of five single NPs obtained by dark field microspectroscopy.[36]

microscope image of some of the core−shells used. The thickness of the gold has to be tuned so that the plasmon resonance obtained enhances the field at the level of the fluorescent emitters at the wavelength of the depletion beam (780 nm in our STED microscope).[32] At the same time, the plasmon resonance must affect the emission properties of the dye as little as possible.[31] For the 60 nm radius cores, the plasmon resonance of the core−shell is slightly higher than 780 nm with a 20 nm thick gold shell. The spectral properties of the core−shells in the conditions used for the STED measurements can be found in Figure 1b. The red curve corresponds to the emission of the ATTO 647N in the silica core and matches well the emission peaking around 670 nm of the dye alone. The gray

dx.doi.org/10.1021/nl5014103 | Nano Lett. 2014, 14, 4449−4453

curves correspond each to the scattering cross section of a single core−shell structure, measured by dark field microscopy.[36] The peak of scattering cross section indicates the position of the dipolar plasmon resonance, red-shifted compared to the emission of the dye, to lead to field enhancement mostly at the depletion wavelength, and to minimize the modification of the fluorescence emission rate. Note that, regardless of the position of the LSPR, dyes placed within ≈5 nm of the metal have their fluorescence quenched. However, with the core−shells used here, most of the dyes should be found away from the metallic shell. The dark-field spectra also show that the optical properties change slightly from one core−shell to another, which is a consequence of the inhomogeneous size and shape distribution of the NPs produced by chemical means. The bare cores and the core−shells are then diluted and drop cast on coverslips, and the solvent is left to evaporate. The dilution is adjusted to ensure that the coverslip presents an average distance between single NP of the order of a couple of micrometers. The side of coverslip with the particles is immersed in index matching oil (Leica Type F, index n = 1.518) and placed in contact with a microscope glass slide. The index matching oil is used to minimize bleaching and backscattering of the depletion laser beam. Images of the NPs are taken on our inverted STED microscope, through the coverslip. The STED experimental setup is presented in the Supporting Information and is similar to that used in refs 9 and 40.

The characterization method used is illustrated in Figure 2 by the case of one single core−shell, pumped in standard conditions, for a depletion power density at the focal plane of the microscope objective of 2.3 MW·cm^{-2}.[41] Images of the NPs are then acquired, first in confocal mode—depletion beam off—and then in FLIM-STED mode. In the latter, a fluorescence decay trace is obtained for each pixel. Figure 2a shows the time trace obtained when integrating the information on all the pixels from the STED-FLIM image of one single core−shell structure, presented in Figure 2c. The time trace has two main features: an exponential decay corresponding to the fluorescence of ATTO 647N (indicated by the dashed line to guide the eye); and a sharp, intense and short peak close to the onset of the fluorescence (≈0.3 ns: the depletion pulse reaches the sample shortly after the pump pulse). To understand the origin of this peak, we have acquired the spectrum of the light collected when only the pump beam is used (inset in Figure 2a, red curve), and when only the depletion beam is used, the pump beam being switched off (inset in Figure 2a, black curve). When only the pump beam is used, the spectrum obtained corresponds well to the fluorescence of ATTO 647N, filtered by the fluorescence band-pass filter used in the microscope. When only the STED beam is used, we obtain a flat spectrum in the range of the band-pass filter. We attribute this to the luminescence of the gold shell of the NPs, probably excited by two-photon absorption of the STED beam:[42,43] the relationship between excitation intensity and parasitic luminescence is quadratic, as shown in the Supporting Information, Figure S3. The temporal decay measured on the bare cores at similar depletion power did not show this instantaneous peak. A much smaller peak at the wavelength of the depletion laser (780 nm) is also present. One effect of the presence of this gold luminescence is the sharp peak visible in the time trace in Figure 2. The second effect is that, in the STED images, reconstructed from the lifetime information, the depletion doughnut produces light that is detected as well. Figure 2b

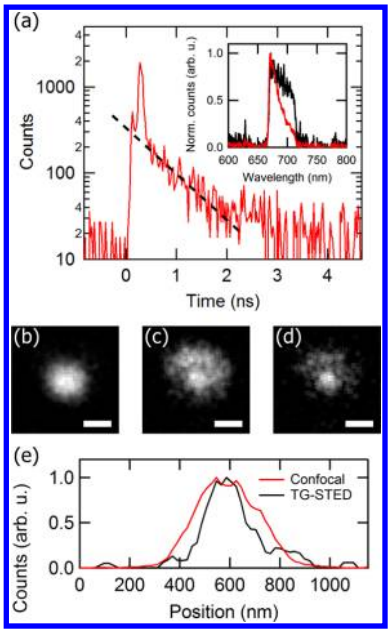

Figure 2. Processing of the images—time gating of FLIM images. (a) Time trace obtained by accumulating all the individual lifetime traces of each pixel of a FLIM image of one single NP (shown in c). The dashed line is a guide to the eye showing the characteristic decay of the fluorescence of the ATTO dye used. The sharp peak occurring 0.3 ns after the onset of the fluorescence corresponds to luminescence emission from the gold shell. Inset: spectra of the light collected by the microscope when only the pump beam is used (red) and when only the STED beam is used (black). The spectra, obtained with different integration times, have been normalized. (b) Confocal image of the NP. (c) Raw STED image of the same NP, acquired with a STED power density at the focal plane of 2.3 MW·cm^{-2}. (d) Time-gated STED image of the NP, reconstructing the image from detection events recorded after the sharp gold luminescence peak seen in (a). For (b), (c), and (d) the color scale is set between 0 and the maximum intensity, and the scale bars represent 300 nm. (e) Horizontal line profiles taken across the confocal (red curve) and time-gated STED (black curve) images. Both profiles have been normalized to allow for an easier comparison.

presents the confocal image of one core−shell NP—only the pump beam is used to excite the NP. Figure 2c is the image reconstituted from the lifetime information on the same NP, acquired subsequently to Figure 2b, when both pump and depletion beams are used. The image in STED mode is clearly not improved compared to the confocal case, due to the parasitic contribution of the gold luminescence excited by the depletion beam. To mitigate the effect of the gold luminescence, we timegate the image by integrating the lifetime signal measured only after the gold luminescence has decayed, in Figure 2a after 0.4 ns. Figure 2d shows the time gated image corresponding to Figure 2c: most of the contribution of the gold luminescence has been removed, leaving an image with improved resolution.

Then, for each NP studied, the same procedure is applied: confocal image followed by STED-FLIM image. The latter is time-gated to minimize the effect of gold luminescence. After this, horizontal profiles taken across the center of the image spots are fitted to a Gaussian model. The full-width at half-maximum of the fit is taken as a measurement of the resolution obtained, and the improvement of resolution χ calculated as $\chi = 100\cdot(1 - W_{STED}/W_{Conf})$, with W_{STED} and W_{Conf} the resolution in STED or confocal mode, respectively. Note that the ratio

dx.doi.org/10.1021/nl5014103 | Nano Lett. 2014, 14, 4449−4453

W_{STED}/W_{Conf} has been denoted as Γ_{res}^{-1} in a previous work,[31] and we will keep this notation below.

Figure 3 compares percentage improvement in resolution obtained for bare cores (blue disks) and for core−shells (black dotted circles), for varying depletion power. The raw fwhm measured can be found in the Supporting Information, Figure S4. For the bare cores, the improvement in resolution increases until it reaches its maximum, around 60%, which corresponds to a resolution close to the size of the NPs. In the case of the core−shells, the resolution increases faster with increasing depletion power density. Above 3.5 MW·cm^{-2}, there are clear signs of degradation of all the core−shells, which we attribute to the heating of the gold shell by the STED beam. For depletion powers between 2.5 MW·cm^{-2} and 3.5 MW·cm^{-2}, some particles also show signs of degradation after interacting with the STED beam, with ∼10% of particles exhibiting damage at the low end of this range and up to a few tens of percent at the top end. This effect could be mitigated by modifying the depletion or scanning conditions, with a rapid scanning of the depletion beam rather than a displacement of the sample, in order to leave more time for the heat generated to diffuse away from the NPs as done, e.g., in ref 44.

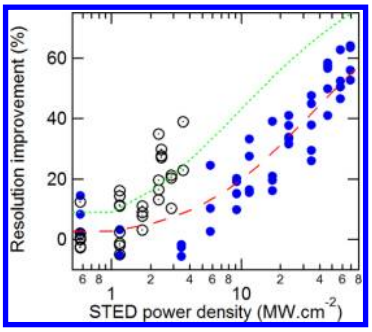

Figure 3. Resolution improvement using core−shell NPs, as a function of the STED depletion power density used. Blue disks: bare doped silica cores only. Black dotted circles: core−shell nanoparticles. The red dashed (respectively green dotted) line is a least-square fit of the bare silica (respectively core−shell) data as described on the text.

Following the notations used in ref 31, the percentage resolution improvement in resolution χ takes the functional form

$$\chi = 100\cdot(1 - \Gamma_{res}^{-1}) = 100\cdot\left(1 - \frac{1}{\sqrt{1 + \Gamma_p(P_{STED}/P_{sat})}}\right) \quad (1)$$

Of course, in the case of the bare cores, $\Gamma_p = 1$. A least-square fit of the data to this function is performed and shown in Figure 3 as a red dashed line for the bare cores and a green dotted line for the core−shells. For the bare cores (respectively the core−shells), the quantity $(1/P_{sat})$ takes the value 0.056 ± 0.004 MW^{-1}·cm^2 (respectively (Γ_p/P_{sat}) = 0.21 ± 0.03 MW^{-1}·cm^2), leading to a ratio of Γ_p = 3.8 ± 0.8. Thus, with the core−shell nanoparticles, a given resolution improvement in STED is obtained with an intensity ∼4 times smaller than that necessary with the bare cores. These results, albeit obtained on NPs of a size not yet optimal for labeling of biological tissues, validates the concept of NP-STED:[32] the addition of a plasmonic cavity to a dye enhances the effect of the depletion beam used and hence lowers the depletion powers required to achieve resolution improvement.

We compared the measured resolution with that deduced from numerical simulations, as described in refs 31, 32, and 38, for the geometrical parameters extracted from the TEM images. As explained in ref 38, since the doughnut beam used in STED imaging has a true zero at its center, it *does not* have an electric dipole moment. Accordingly, the field enhancement level shifts from the enhancement appropriate to the next highest multipole moment in the beam (an electric quadrupolar in the current case) for the case where the beam is centered on the NP to the enhancement appropriate to the electric dipole moment as the doughnut beam is scanned away from the metal NP. Mie-type calculations show that the average intensity enhancement within the core of the nanoshell, as a function of the scan coordinate, is roughly 4. Judging from the emission data and dark-field images (see Figure 1), we estimate the decay rate enhancement to be negligible. Thus, the intensity reduction predicted theoretically is close to the measured value. The slight theory−experiment discrepancy could be due to a number of factors, such as the possibility that the actual geometrical parameters of the core−shells differ from those deduced from the TEM images or that the roughness of the metallic shell plays a role. More information about the evolution of the field enhancement when the doughnut is scanned over the NP is shown in the Supporting Information, section on additional data on the theoretical modeling. In the present article we observe that the depletion power required for the specific hybrid NPs used is four times less than for the same labels without gold. Earlier calculations suggest that up to 2 orders of magnitude reduction could be achieved for smaller dimensions of core−shell structures, for which the near-field enhancement is higher.[32] However, to this date, the reliable synthesis of hybrid NPs with dimensions in the tens of nanometer range remains challenging, and progress in that field will be required to access the full potential of NP-STED.

In conclusion, in this article we have imaged nanoparticles with 120 nm diameter spherical cores of silica doped with ATTO 647N covered by a 20 nm gold shell with our STED-FLIM nanoscope. We have observed that the improvement of resolution in STED mode for the core−shell NPs requires four times less depletion power than required for the same particles without the gold shell. These results validate the concept of NP-STED and open the door to obtain even better performances with smaller nanoparticles. The NP-STED performance could be further improved in many ways, for instance by using continuous wave depletion beams:[6,7] with a cw STED beam the luminescence of the gold we observed would be greatly reduced, due to the lower associated instantaneous powers. Also, further studies will be required to assess the effect of NP-STED on bleaching and to understand fully the interplay of parameters such as change in the decay rate of the dye induced by the plasmon resonance and field enhancement at the STED wavelength. Reducing the power needed to reach STED resolution enhancement is particularly useful for the recent development of parallel STED schemes, using several doughnuts at the same time, which increases the speed of the measurements but also requires more laser power to generate the depletion beams[45]—a drawback that could be alleviated by NP-STED.

■ ASSOCIATED CONTENT

Supporting Information

STED microscope—experimental configuration, resolution improvement: STED vs. NP-STED, depletion curve, lumines-

dx.doi.org/10.1021/nl5014103 | Nano Lett. 2014, 14, 4449−4453

cence of gold, and additional data on the resolution and the theoretical modeling. This material is available free of charge via the Internet at http://pubs.acs.org.

AUTHOR INFORMATION

Corresponding Author

*E-mail: yannick.sonnefraud@neel.cnrs.fr.

Notes

The authors declare no competing financial interest.

ACKNOWLEDGMENTS

The authors acknowledge support from the Leverhulme Research Project Grant *Nanoparticle assisted super-resolution microscopy for live cell imaging*, MRC grant MR/K015834/1, and thank E. Auksorius and M. Lenz for their help in the initial stages of the project. M.R.F. acknowledges support from an Alexander von Humboldt Foundation fellowship. Y. Sivan acknowledges support by the Royal Society Newton fellowship Alumni program, the ESF (European Science Foundation) as well as by INNI (Isreal Nano initiative) via an FTA (Focus Technology Area) grant. H.G.S. acknowledges support from the EPSRC Case studentship with the Diamond Trading Company (De Beers Technology). Y. Sonnefraud acknowledges support by the UK Engineering and Physical Sciences Research Council (EPSRC). Y. Sonnefraud and S.A.M. acknowledge support from the EOARD, Grant No. FA8659-09-1-3080. The authors would like to thank the anonymous reviewers of this article, whose comments have allowed to improve it significantly.

REFERENCES

(1) Hell, S. W.; Wichmann, J. *Opt. Lett.* **1994**, *19*, 780−782.
(2) Klar, T. A.; Hell, S. W. *Opt. Lett.* **1999**, *24*, 954−956.
(3) Klar, T. A.; Jakobs, S.; Dyba, M.; Egner, A.; Hell, S. W. *Proc. Natl. Acad. Sci. U.S.A.* **2000**, *97*, 8206−8210.
(4) Willig, K. I.; Rizzoli, S. O.; Westphal, V.; Jahn, R.; Hell, S. W. *Nature* **2006**, *440*, 935−939.
(5) Eggeling, C.; Ringemann, C.; Medda, R.; Schwarzmann, G.; Sandhoff, K.; Polyakova, S.; Belov, V. N.; Hein, B.; von Middendorff, C.; Schönle, A.; Hell, S. W. *Nature* **2009**, *457*, 1159.
(6) Willig, K. I.; Harke, B.; Medda, R.; Hell, S. W. *Nat. Methods* **2007**, *4*, 915.
(7) Moneron, G.; Medda, R.; Hein, B.; Giske, A.; Westphal, V.; Hell, S. W. *Opt. Express* **2010**, *18*, 1302−1309.
(8) Schrof, S.; Staudt, T.; Rittweger, E.; Wittenmayer, N.; Dresbach, T.; Engelhardt, J.; Hell, S. W. *Opt. Express* **2011**, *19*, 8066−8072.
(9) Auksorius, E.; Boruah, B. R.; Dunsby, C.; Lanigan, P. M. P.; Kennedy, G.; Neil, M. A. A.; French, P. M. W. *Opt. Lett.* **2008**, *33*, 113−115.
(10) Moffitt, J. R.; Osseforth, C.; Michaelis, J. *Opt. Express* **2011**, *19*, 4242−4254.
(11) Vicidomini, G.; Moneron, G.; Han, K. Y.; Westphal, V.; Ta, H.; Reuss, M.; Engelhardt, J.; Eggeling, C.; Hell, S. W. *Nat. Methods* **2011**, *8*, 571−573.
(12) Galiani, S.; Harke, B.; Vicidomini, G.; Lignani, G.; Benfenati, F.; Diaspro, A.; Bianchini, P. *Opt. Express* **2012**, *20*, 7362−7374.
(13) Hell, S. W. *Science* **2007**, *316*, 1153−1158.
(14) Hell, S.; Kroug, M. *Appl. Phys. B: Laser Opt.* **1995**, *60*, 495−497.
(15) Gustafsson, M. G. L. *J. Microsc.* **2000**, *198*, 82−87.
(16) Gustafsson, M. G. L. *Proc. Natl. Acad. Sci. U.S.A.* **2005**, *102*, 13081−13086.
(17) Hofmann, M.; Eggeling, C.; Jakobs, S.; Hell, S. W. *Proc. Natl. Acad. Sci. U.S.A.* **2005**, *102*, 17565−17569.
(18) Betzig, E.; Patterson, G. H.; Sougrat, R.; Lindwasser, O. W.; Olenych, S.; Bonifacino, J. S.; Davidson, M. W.; Lippincott-Schwartz, J.; Hess, H. F. *Science* **2006**, *313*, 1642−1645.
(19) Rust, M. J.; Bates, M.; Zhuang, X. *Nat. Methods* **2006**, *3*, 793−796.
(20) Fujita, K.; Kobayashi, M.; Kawano, S.; Yamanaka, M.; Kawata, S. *Phys. Rev. Lett.* **2007**, *99*, 228105.
(21) Hein, B.; Willig, K. I.; Wurm, C. A.; Westphal, V.; Jakobs, S.; Hell, S. W. *Biophys. J.* **2010**, *98*, 158−163.
(22) Berning, S.; Willig, K. I.; Steffens, H.; Dibaj, P.; Hell, S. W. *Science* **2012**, *335*, 551.
(23) Lukinavicius, G.; et al. *Nat. Chem.* **2013**, *5*, 132−139.
(24) Maier, S. A. *Plasmonics: Fundamentals and Applications*; Springer-Verlag Inc.: New York, 2007.
(25) Sonnefraud, Y.; Leen Koh, A.; McComb, D.; Maier, S. *Laser Photonics Rev.* **2012**, *6*, 277.
(26) Willets, K. A.; Duyne, R. P. V. *Annu. Rev. Phys. Chem.* **2008**, *58*, 267−297.
(27) Neubrech, F.; Pucci, A.; Cornelius, T. W.; Karim, S.; García-Etxarri, A.; Aizpurua, J. *Phys. Rev. Lett.* **2008**, *101*, 157403.
(28) Giannini, V.; Fernández-Domínguez, A. I.; Sonnefraud, Y.; Roschuk, T.; Fernández-García, R.; Maier, S. A. *Small* **2010**, *6*, 2498.
(29) Kinkhabwala, A.; Yu, Z.; Fan, S.; Avlasevich, Y.; Mullen, K.; Moerner, W. E. *Nat. Photonics* **2009**, *3*, 654.
(30) Liu, Z., Ed. *Plasmonics and super resolution imaging*; PAN Stanford Press: Singapore, 2014.
(31) Sivan, Y. *Appl. Phys. Lett.* **2012**, *101*, 021111.
(32) Sivan, Y.; Sonnefraud, Y.; Kéna-Cohen, S.; Pendry, J. B.; Maier, S. A. *ACS Nano* **2012**, *6*, 5291−5296.
(33) Balzarotti, F.; Stefani, F. D. *ACS Nano* **2012**, *6*, 4580−4584.
(34) Maier, S. A. *Opt. Express* **2006**, *14*, 1957−1964.
(35) Zhang, H.; Zhao, M.; Peng, L. *Optics Express* **2011**, *19*, 24783−24794.
(36) Lei, D. Y.; Fernández-Domínguez, A. I.; Sonnefraud, Y.; Appavoo, K.; Haglund, R. F.; Pendry, J. B.; Maier, S. A. *ACS Nano* **2012**, *6*, 1380−1386.
(37) Oldenburg, S. J.; Averitt, R. D.; Westcott, S. L.; Halas, N. J. *Chem. Phys. Lett.* **1998**, *288*, 243−247.
(38) Foreman, M. R.; Sivan, Y.; Maier, S. A.; Török, P. *Phys. Rev. B* **2012**, *86*, 155441.
(39) Ow, H.; Larson, D. R.; Srivastava, M.; Baird, B. A.; Webb, W. W.; Wiesner, U. *Nano Lett.* **2005**, *5*, 113 ; PMID: 15792423.
(40) Lenz, M. O.; Sinclair, H. G.; Savell, A.; Clegg, J. H.; Brown, A. C. N.; Davis, D. M.; Dunsby, C.; Neil, M. A. A.; French, P. M. W. *J. Biophotonics* **2014**, *7*, 29−36.
(41) The estimation of the power density at the focal plane of the microscope objective is done as follows: first the quasi-cw power of the 80 MHz pulse train is measured just before the microscope. Then we make the approximation that it is focused on a disk of diameter d calculated by the expression $d = (\lambda/2\mathrm{NA})$, with $\lambda = 780$ nm the wavelength of the STED beam, and NA = 1.4 the numerical aperture of the microscope objective. The result is multiplied by 0.7 to account for a transmission of the objective of ≈70%.
(42) Beversluis, M. R.; Bouhelier, A.; Novotny, L. *Phys. Rev. B* **2003**, *68*, 115433.
(43) Park, J.; Estrada, A.; Sharp, K.; Sang, K.; Schwartz, J. A.; Smith, D. K.; Coleman, C.; Payne, J. D.; Korgel, B. A.; Dunn, A. K.; Tunnell, J. W. *Opt. Express* **2008**, *16*, 1590−1599.
(44) Chu, S.-W.; Su, T.-Y.; Oketani, R.; Huang, Y.-T.; Wu, H.-Y.; Yonemaru, Y.; Yamanaka, M.; Lee, H.; Zhuo, G.-Y.; Lee, M.-Y.; Kawata, S.; Fujita, K. *Phys. Rev. Lett.* **2014**, *112*, 017402.
(45) Chmyrov, A.; Keller, J.; Grotjohann, T.; Ratz, M.; d'Este, E.; Jakobs, S.; Eggeling, C.; Hell, S. W. *Nat. Methods* **2013**, *10*, 737.